The Rice Actin-Binding Protein RMD Regulates Light-Dependent Shoot Gravitropism[1][OPEN]

Yu Song,[a] Gang Li,[b] Jacqueline Nowak,[c,d,e] Xiaoqing Zhang,[a] Dongbei Xu,[a] Xiujuan Yang,[b] Guoqiang Huang,[a] Wanqi Liang,[a] Litao Yang,[a] Canhua Wang,[a] Vincent Bulone,[b] Zoran Nikoloski,[c,d] Jianping Hu,[f] Staffan Persson,[a,e] and Dabing Zhang[a,b,2,3]

[a]The University of Adelaide-Shanghai Jiao Tong University Joint Laboratory for Plant Science and Breeding, School of Life Sciences and Biotechnology, Shanghai Jiao Tong University, 200240 China
[b]School of Agriculture, Food and Wine, University of Adelaide, Urrbrae, South Australia 5064, Australia
[c]Systems Biology and Mathematical Modeling Group, Max Planck Institute of Molecular Plant Physiology, 14476 Potsdam-Golm, Germany
[d]Bioinformatics Group, Institute of Biochemistry and Biology, University of Potsdam, 14476 Potsdam-Golm, Germany
[e]Department of Energy Plant Research Laboratory, Michigan State University, East Lansing, Michigan 48824
[f]School of Biosciences, University of Melbourne, Parkville Victoria 3010, Melbourne, Australia

ORCID IDs: 0000-0002-1744-5220 (G.L.); 0000-0002-2881-7384 (J.N.); 0000-0002-6103-5704 (G.H.); 0000-0002-9938-5793 (W.L.); 0000-0002-4515-5722 (L.Y.); 0000-0003-2671-6763 (Z.N.); 0000-0002-4635-4299 (J.H.); 0000-0002-6377-5132 (S.P.); 0000-0002-1764-2929 (D.Z.).

Light and gravity are two key determinants in orientating plant stems for proper growth and development. The organization and dynamics of the actin cytoskeleton are essential for cell biology and critically regulated by actin-binding proteins. However, the role of actin cytoskeleton in shoot negative gravitropism remains controversial. In this work, we report that the actin-binding protein Rice Morphology Determinant (RMD) promotes reorganization of the actin cytoskeleton in rice (*Oryza sativa*) shoots. The changes in actin organization are associated with the ability of the rice shoots to respond to negative gravitropism. Here, light-grown *rmd* mutant shoots exhibited agravitropic phenotypes. By contrast, etiolated *rmd* shoots displayed normal negative shoot gravitropism. Furthermore, we show that RMD maintains an actin configuration that promotes statolith mobility in gravisensing endodermal cells, and for proper auxin distribution in light-grown, but not dark-grown, shoots. *RMD* gene expression is diurnally controlled and directly repressed by the phytochrome-interacting factor-like protein OsPIL16. Consequently, overexpression of *OsPIL16* led to gravisensing and actin patterning defects that phenocopied the *rmd* mutant. Our findings outline a mechanism that links light signaling and gravity perception for straight shoot growth in rice.

Light and gravity are two key determinants for plant growth and development, as they drive the establishment of the above- and below-ground developmental axes of a plant. This is especially important at the seedling establishment stage, a time when plants are sensitive to light and gravity (Gommers and Monte, 2018). However, how plants coordinate light and gravity perception and signaling is not well understood.

"Gravitropism" is the process by which plants adjust their growth in response to gravity, ensuring that shoots grow upward and roots grow downward. Gravitropism consists of gravisensing, signal initiation, and transduction, and asymmetric cell growth (Blancaflor and Masson, 2003). In root columella cells and shoot endodermal cells, starch-filled amyloplasts are considered as statoliths. (Blancaflor and Masson, 2003; Morita, 2010). Statoliths sediment according to the gravity vector to propagate gravitropic signals that are converted into biochemical and physiological outputs; for example, redistribution of auxin (Kiss, 2000). Although the root gravitropic response is relatively

[1]This work was supported by the National Key Research and Development Program of China (grant no. 2016YFD0100804), the National Natural Science Foundation of China (grant no. 31430009), the Innovative Research Team, Ministry of Education, and 111 Project (grant no. B14016), the Science and Technology Commission of Shanghai Municipality (grant no. 13JC1408200), the China Scholarship Council (CSC grant no. 201506230050), the Australian Research Council Future Fellowship (grant no. FT160100218 to S.P.), and the University of Melbourne International Research and Research Training Fund-Research Network and Consortia (grant to S.P.).

[2]Author for contact: zhangdb@sjtu.edu.cn.
[3]Senior author.
The author responsible for distribution of materials integral to the findings presented in this article in accordance with the policy described in the Instructions for Authors (www.plantphysiol.org) is: Dabing Zhang (zhangdb@sjtu.edu.cn).

D.Z., S.P., Y.S., J.H., and V.B. designed the project; Y.S., G.L., J.N., X.Z., D.X., X.Y., and G.H. performed the experiments; Y.S., G.L., J.N., Z.N., X.Z., D.X., X.Y., G.H., W.L., C.W., L.Y., D.Z., and S.P. analyzed the data; Y.S., D.Z., S.P., J.H., J.N., and Z.N. co-wrote the article; all authors discussed the results and commented on the article.
[OPEN]Articles can be viewed without a subscription.
www.plantphysiol.org/cgi/doi/10.1104/pp.19.00497

well understood, the molecular mechanisms that underpin shoot negative gravitropic responses remain ill-defined. However, studies of shoot negative gravitropic mutants have shed some light on this process. For example, mutations in the transcription factors (TFs) *SCARECROW* and *SHORT-ROOT*, which are essential for the development of endodermis, caused agravitropic responses in Arabidopsis (*Arabidopsis thaliana*) stems (Fukaki et al., 1998). Shoot gravitropism3 (SGR3), a syntaxin, together with SNARE protein ZIG (ZIG-ZAG), forms a SNARE complex, which positively mediates shoot negative gravitropism via vesicle transport (Yano et al., 2003). In Arabidopsis, hypocotyls of starch excess (*sex1*) mutant displayed increased gravity response, and the amyloplasts were twice as big as those of wild type in the endodermal cells (Vitha et al., 2007). However, root gravitropic response, as well as amyloplast sedimentation in root columella cells, of sex1 was similar to that of wild type (Vitha et al., 2007). Similarly, inflorescence stems of *shoot gravitropism 1* (*sgr3*), *sgr5*, and *sgr6* exhibited defective gravitropic response, but gravitropic responses of hypocotyls and roots were normal (Tasaka et al., 1999), indicating that gravitropic responses occur via different mechanisms in distinct organs (Mirza et al., 1984; Hobbie and Estelle, 1995; Fukaki et al., 1996, 1998; Yamauchi et al., 1997; Morita et al., 2006).

The gravitropic response system interacts with the response pathways of other environmental signals. For example, light and gravitropism intersect in plant shoots. In Arabidopsis, dark-grown hypocotyls show strong negative gravitropism, but light-grown hypocotyls display random growth orientation under red or far-red light conditions (Poppe et al., 1996). Light inhibition of negative gravitropism in hypocotyls is mediated by phytochromes (Poppe et al., 1996; Robson and Smith, 1996). For example, the tomato (*Solanum lycopersicum*) mutant of *LAZY-2* (*LZ2*, not yet cloned) grew downward in a phytochrome-dependent manner when exposed to white light, but displayed normal gravitropic response in the dark (Gaiser and Lomax, 1993; Behringer and Lomax, 1999). In addition, phytochrome-interacting factors (PIFs) positively regulate shoot negative gravitropism by controlling endodermal amyloplast development in Arabidopsis etiolated hypocotyls (Kim et al., 2011). Despite these findings, molecular mechanisms on how plants coordinate light and gravity perception and signal transduction are not well defined.

An intact and dynamic actin cytoskeleton is thought to be important for plants to respond to gravity; however, pharmaceutical treatment and mutant analyses have yielded conflicting results (Yamamoto and Kiss, 2002; Hou et al., 2003; Palmieri and Kiss, 2005). In Arabidopsis shoots, pharmacological disruption of the F-actin cytoskeleton formation by Latrunculin B (LatB) led to increased gravitropic response (Yamamoto and Kiss, 2002). However, other studies have questioned the need for an intact F-actin network for graviperception in inflorescence stems (Hou et al., 2003; Saito et al., 2005), and Lat-B treatment caused reduced amyloplast mobility in Arabidopsis endodermal cells (Palmieri and Kiss, 2005). Previously, we showed that the actin cytoskeleton in rice (*Oryza sativa*) is controlled by Rice Morphology Determinant (RMD, also called "BUI1"), a type-II formin protein specifying rice morphology by regulating actin nucleation and organization (Zhang et al., 2011). RMD also regulates actin dynamics and auxin homeostasis during root cell elongation and growth (Li et al., 2014), as well as pollen tube development (Li et al., 2018), and it is required for crown root angle in response to P starvation (Huang et al., 2018). Here, we show that RMD promotes shoot negative gravitropism by regulating actin organization and amyloplast sedimentation in the endodermis of light-grown shoots. *RMD* gene expression is controlled by the diurnally active phytochrome-interacting factor-like protein OsPIL16. We have thus uncovered a mechanism by which RMD is involved in controlling shoot negative gravitropism in a light-dependent manner.

RESULTS

RMD Is Required for Rice Shoots to Grow Upright in the Light

Our previous studies indicated that the actin-binding protein RMD is a vital regulator of rice morphology (Yang et al., 2011; Zhang et al., 2011). A prominent phenotype of the *rmd* mutants is that their shoots tend to be bent rather than straight as observed in wild type (Yang et al., 2011; Zhang et al., 2011). This observation indicates a function of RMD during rice seedling establishment and vertical growth maintenance. To quantify the shoot bending of *rmd* mutant seedlings, we measured the shoot deviation from straight growth in two null alleles of *RMD*, *rmd-1* and *rmd-2* (Zhang et al., 2011). Mean values of the angle (θ) between the direction of growth and the longitudinal axis were compared. In light conditions, >85% of *rmd-2* displayed a clear agravitropic phenotype, 37.65% at 0° to 20°, 39.51% at 20° to 40°, and 8.02% at 40° to 60° (Fig. 1A; Supplemental Fig. S1). By contrast, etiolated *rmd-1* and *rmd-2* seedlings grew their shoots straight upward just like that of wild type (Fig. 1B). These observations indicated that the shoot phenotype of *rmd* mutants is light-specific. Further, an *rmd-2* mutant complemented by an estradiol-inducible *pLex*::*RMD-RFP* transgene (Li et al., 2014) showed no shoot bending phenotype when grown in the light on estradiol-containing media (Supplemental Fig. S2A), confirming that the shoot-bending phenotype in the mutant is due to the lack of a functional RMD.

To investigate whether the shoot bending of *rmd* mutants was due to differential cell elongation, we performed semisection assays to analyze cell length of wild-type and *rmd-2* shoots. In light-grown *rmd-2* sheaths, cell lengths at the inward side of the bent

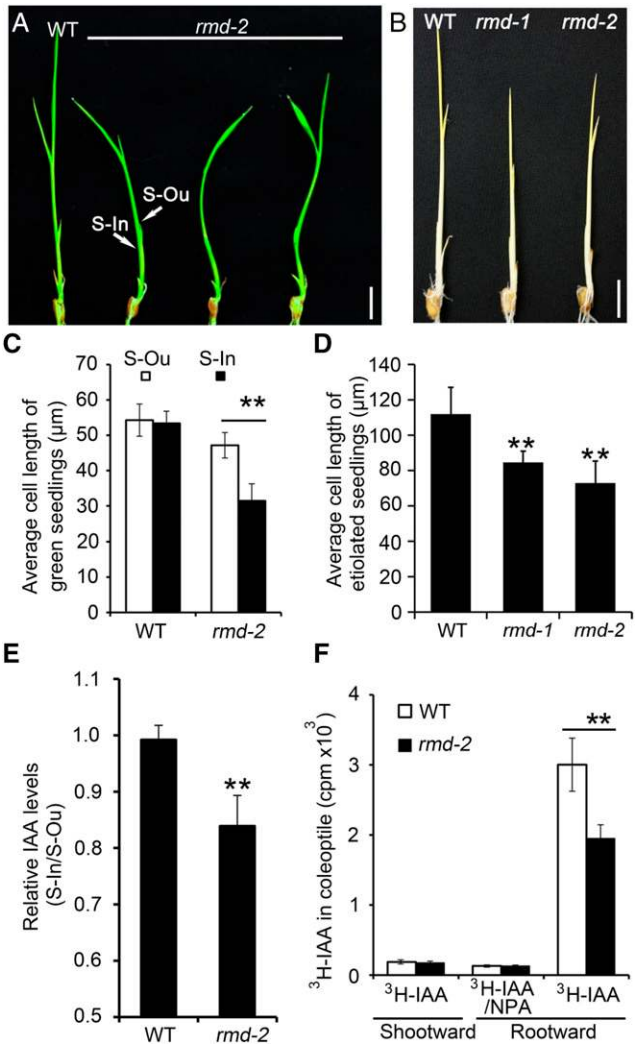

Figure 1. The *rmd* mutant displays light-dependent agravitropic growth and aberrant auxin homeostasis in the shoot. A, Shoots of 5-d–old seedlings after germination under light/dark cycle. Scale bar = 1 cm. B, Shoots of 3-d–old seedlings after germination in darkness. Scale bar = 1 cm. C, S-Ou (outer side of leaf sheaths) and S-In (inner side of leaf sheaths) cell length in light-grown wild-type (WT; $n > 120$ cells from 10 shoots) and *rmd-2* ($n > 141$ cells from 12 shoots) seedlings. Results are presented as means ± SD. Student's *t* test: $^{**}P < 0.01$. D, Cell length of sheaths in etiolated wild-type ($n = 45$), *rmd-1* ($n = 48$), and *rmd-2* ($n = 40$) shoots. Data were analyzed by conducting both *t* test and ANOVA. Results are presented as means ± SD. $^{**}P < 0.01$. E, The ratio between IAA levels in S-In versus S-Ou in shoots without apex. Results are presented as means ± SD. Student's *t* test: $^{**}P < 0.01$. F, Coleoptile auxin polar transport assays. NPA (1-N-Naphthylphthalamic acid; 10 μM) was applied to inhibit auxin transport ($n = 3$). Results are presented as means ± SD. Student's *t* test: $^{**}P < 0.01$.

region were significantly shorter (~34%) than those at the outward bending side. On the contrary, no significant differences in cell lengths were found between opposite sides of wild-type sheaths (Fig. 1C). Despite the lack of a shoot-bending phenotype in dark-grown *rmd-2*, cell lengths were overall shorter in the mutant than in the wild type (Fig. 1D), consistent with the fact that *rmd* mutants have shorter hypocotyls (Zhang et al., 2011). These results suggested that the shoot-bending phenotype in *rmd* is due to asymmetric cell elongation in light-grown shoots.

RMD Is Required for Auxin Transport and Distribution in the Shoot

The downward growth of the *rmd* mutant seedlings is comparable to that of the prostrate growth of the maize (*Zea mays*) *lazy1* (*la1*) mutant, that is affected in polar auxin distribution (Dong et al., 2013). With the purpose of determining whether auxin homeostasis is perturbed in *rmd* shoots, which might result in the observed asymmetric cell elongation, we measured indole-3-acetic acid (IAA) levels in tissues from the inward and outward sides of the bending region in shoots. Results showed that the IAA level from the inward side was lower (2.78 pg/mg) than that of the outward side (3.31 pg/mg) in light-grown *rmd-2* shoots, whereas no differences in IAA levels were observed from the two opposite shoot sides in wild type (Fig. 1E).

To directly measure the polar auxin transport capacity of the plant, we compared rootward IAA transport in coleoptiles between wild type and *rmd-2* mutants. We found that rootward polar auxin transport was 1.95 ± 10^3 cpm (counts per minute) in *rmd-2* mutants, and significantly reduced from the 3×10^3 cpm in wild type (Fig. 1F). It is well established that auxin export activity relies on PIN auxin efflux carriers (Ding et al., 2011). Therefore, we next analyzed OsPIN1b localization in the shoot using transgenic lines expressing an OsPIN1b-YFP fusion protein under the control of the native *OsPIN1b* promoter (*ProOsPIN1b*::OsPIN1b-YFP). In leaf sheaths of light-grown plants, we observed that OsPIN1b-YFP was detected in the basal plasma membrane of the cells in wild type, but some were clearly distributed to the lateral sides of *rmd-2* (Supplemental Fig. S2B). By contrast, OsPIN1b displayed very similar localization patterns in etiolated shoot cells of *rmd-2* and wild-type seedlings (Supplemental Fig. S2C). These data indicated that RMD is important for polar OsPIN1b localization, and proper auxin homeostasis, in light-grown rice shoots. The altered auxin distribution in the *rmd* shoots may cause the asymmetrical cell elongation and bent phenotype of light-grown shoots.

The Light-Dependent Phenotype in *rmd* Is Associated with Reduced Gravitropic Response

We hypothesized that the inability of the light-grown *rmd* seedlings to grow straight up was associated with a defect in the gravitropic response. To test this hypothesis, we first selected 2-d–old light-grown wild-type and *rmd-2* mutants to analyze gravitropic responses. At this stage the seedlings do not have any true leaves, which may complicate interpretations. The

results revealed that *rmd-2* displayed a reduced level of the gravitropic response (Supplemental Fig. S3, A and B). Next, we analyzed shoot negative gravitropism of *rmd-2* by reorienting 5-day–old seedlings 90° from their previous growth position at different light conditions. Light-grown *rmd-2* seedlings displayed markedly a reduced shoot gravitropic response after gravity stimulation compared with wild type (Fig. 2, A and B). By contrast, etiolated *rmd-2* mutants exhibited a normal shoot gravitropic response (Fig. 2, C and D).

Endodermal amyloplasts are thought to act as statoliths in shoot negative gravitropism (Morita, 2010). To test whether amyloplast behavior is affected in the *rmd* mutants, we checked the localization of amyloplasts in the endodermal cells using histological analyses. Under light, amyloplasts were distributed at the base of the endodermal cells, in accordance with the gravity vector, in wild-type seedlings (Supplemental Fig. S4A), but exhibited uneven distribution in *rmd-2* (Supplemental Fig. S4A). Indeed, some amyloplasts were visible along the sides, or displaced to the central part, of the endodermal cells in the light-grown *rmd-2* mutants (Supplemental Fig. S4A). This result indicated that RMD promotes amyloplast sedimentation in shoot endodermal cells, which differs from the role of RMD in buffering amyloplast movement in root columella

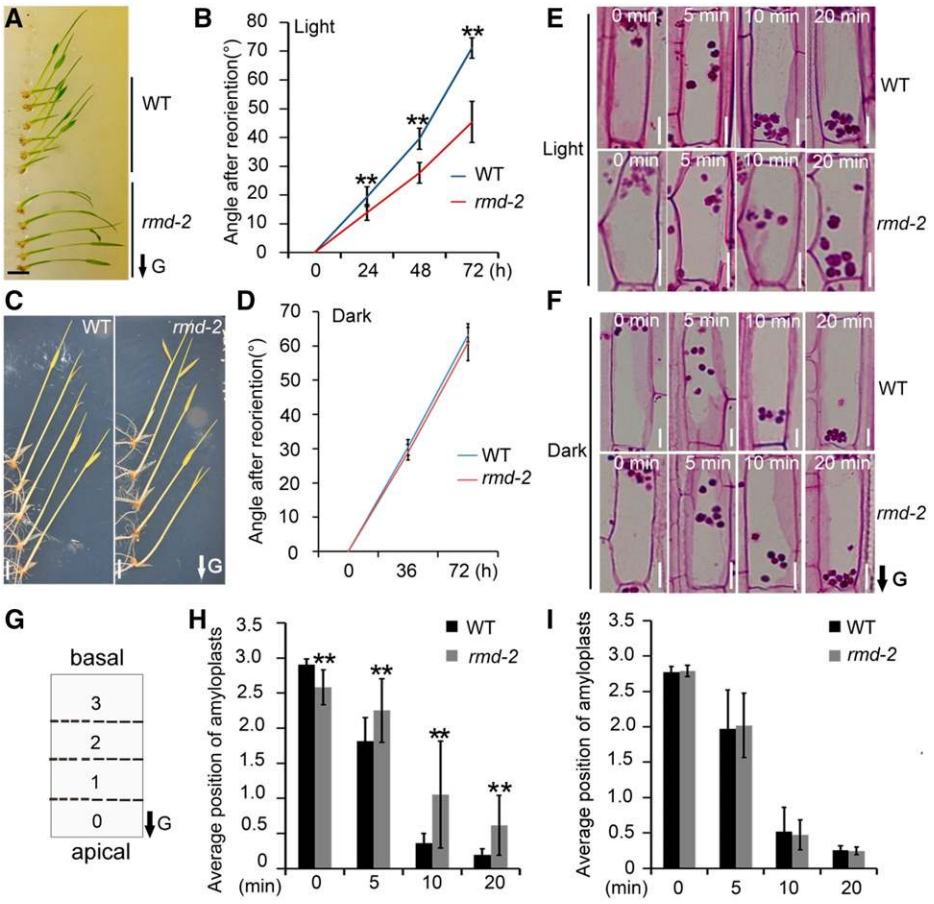

Figure 2. The curved growth of *rmd* shoot is caused by reduced gravisensing under light. A, Seventy-two hours after 5-d–old wild-type (WT) and *rmd-2* seedlings grown under light/dark cycle were reoriented for 90°. Scale bar = 1 cm. B, Kinetic comparison of shoot curved angle between wild type ($n = 14$) and *rmd-2* ($n = 16$) under gravistimulation. Values are means ± SD. Student's *t* test: $^{**}P < 0.01$. C, Seventy-two hours after 5-d–old etiolated wild type ($n = 15$) and *rmd-2* ($n = 15$) were reoriented for 90°. The arrow indicates gravity direction. Scale bar = 1 cm. D, Measurement of curve angle of wild-type ($n = 15$) and *rmd-2* ($n = 15$) etiolated seedlings 72 h after seedlings were reoriented. Values are means ± SD. Student's *t* test. E and F, Comparison of the kinetics of amyloplast sedimentation in shoot endodermal cells between wild type and *rmd* in light-grown (E) and etiolated (F) seedlings. Amyloplasts were stained by periodic acid-Schiff kit after 0, 5, 10, and 20 min of the gravistimulation. Scale bars = 10 μm. The arrow indicates gravity direction. G, Schematic position of amyloplasts in endodermal cells. Each cell is divided into four equal segments, numbered 0–3. Amyloplasts moved from basal to apical after seedlings were inverted and their positions were scored. The arrow indicates gravity direction. H, Average position of amyloplasts (defined in G) in light-grown wild type ($n = 86$ from four shoots) and *rmd-2* ($n = 86$ from four shoots) seedlings at different time points after seedlings were reoriented. Values are means ± SD. Student's *t* test: $^{**}P < 0.01$. I, Average position of amyloplasts (defined in G) in dark-grown wild type ($n = 74$ from four shoots) and *rmd-2* ($n = 74$ from four shoots) seedlings at different time points after seedlings were reoriented. Values (defined in G) are means ± SD.

cells during gravisensing (Huang et al., 2018). The amyloplasts were distributed along the basal part of the endodermal cells in both etiolated *rmd-2* and wild-type plants, consistent with the lack of bent phenotypes of the *rmd* mutants (Supplemental Fig. S4B). These results indicated that the gravitropic defect of *rmd* was associated with amyloplast behavior.

Changes in the gravity vector trigger changes in the localization of amyloplasts (Kiss, 2000). To investigate the dynamics of amyloplasts in *rmd* plants during shoot negative gravitropic response, we performed histochemical analyses to check amyloplast relocalization after seedlings were reoriented. After turning 5-d–old light-grown wild type rice seedlings upside-down, we found that most amyloplasts moved to the basal side of endodermal cells already 10 min after the turn (Fig. 2, E, G, and H). However, the majority of amyloplasts in *rmd-2* failed to reach the basal region of the endodermal cells and instead remained at the central part 10 min after the turn (Fig. 2, E, G, and H). After 20 min, although some of the amyloplasts in *rmd-2* did reach the base of the endodermal cells, many of them still remained scattered in the cells (Fig. 2, E, G, and H). In dark-grown seedlings, however, the dynamics of amyloplasts were very similar in wild type and *rmd-2* after the seedlings were reoriented (Fig. 2, F, G, and I). Thus, we propose that RMD affects shoot negative gravitropism in light-grown rice seedlings and impacts the redistribution and dynamics of amyloplasts in the endodermal cell layers.

Organization of the Actin Cytoskeleton Is Disturbed in the Shoot Endodermis of Light-Grown *rmd* Mutants

Given our previous report that RMD is localized to the chloroplast surface in leaf cells (Zhang et al., 2011) and on the surface of statoliths in root columella cells (Huang et al., 2018), we predicted that the RMD protein may be physically associated with amyloplasts in the shoot. To test this hypothesis, we performed confocal microscopy on rescued *rmd-2* lines that contained the RMD-GFP fusion under the control of the native promoter of *RMD* (Huang et al., 2018; Fig. 3A). Consistent with our previous results (Huang et al., 2018), we found that a functional RMD-GFP localized to distinct organelles, reminiscent of amyloplasts, inside the endodermal cells of rice shoots (Fig. 3, B and C), indicating that RMD was mainly localized to amyloplasts in shoot endodermis.

RMD binds to actin filaments (AFs) in vitro and affects actin organization in roots and pollen tubes (Yang et al., 2011; Zhang et al., 2011; Li et al., 2018). To first assess whether the actin cytoskeleton is important for shoot gravitropism, we transferred germinated wild-type rice seeds to half-strength Murashige and Skoog (MS) liquid medium supplemented with 1 μM of LatB, an actin polymerization inhibitor (Baluška et al., 2001). Light-grown wild-type seedlings grown on LatB showed bent shoot growth or twisted shoots

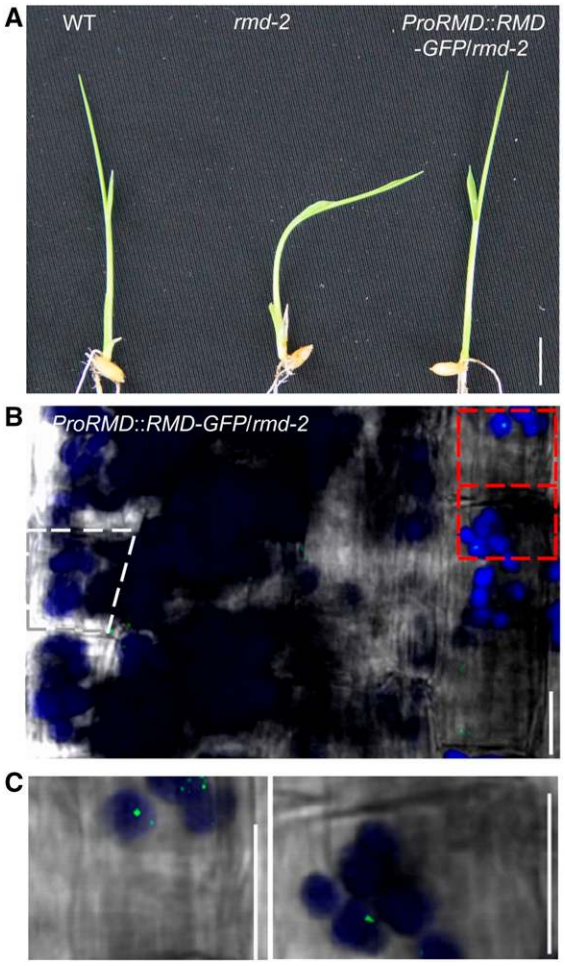

Figure 3. The RMD protein is associated with amyloplasts in the shoot. A, Complementation of the *rmd-2* mutant by *ProRMD*::*RMD-GFP*. B, Intracellular localization of RMD-GFP in shoot endodermal cells. Cy5 (cyan) signals are autofluorescence of amyloplasts. The dotted gray circle indicated the cortex cell. At least 10 lines were checked. C, A magnified view of the area enclosed in the dotted red circle of (B). Scale bars = 1 cm (A) and 10 μm (B and C). WT, wild type.

(Supplemental Fig. S5A), and thus phenocopied the growth of the *rmd* mutants. By contrast, the majority of dark-grown wild-type seedlings grown on LatB-containing medium exhibited normal vertical growth, with less than ~30% seedlings displaying abnormal growth patterns (Supplemental Fig. S5B). LatB-grown wild-type seedlings contained unevenly distributed amyloplasts at the distal end of light-grown endodermal cells (Supplemental Fig. S5C). For LatB-treated etiolated seedlings, we found normal amyloplast sedimentation at the base of the endodermis in vertical growth seedlings. However, amyloplasts displacement to the central part of endodermal cells was observed in bending etiolated seedlings (Supplemental Fig. S5D). These results demonstrate that the abnormal gravitropic perception in *rmd* might be connected to the role of RMD in actin organization under light.

We next reasoned that RMD may influence amyloplast distribution and dynamics through its impact on organization of the actin cytoskeleton in the endodermis. To investigate if actin organization was changed in the *rmd* mutants from wild type in endodermal cells, we stained shoot endodermal cells with AlexaFluor488-phalloidin. Confocal microscopy showed sparser AF abundance and abnormal amyloplast distribution in light-grown *rmd-2* endodermal cells compared with wild type (Fig. 4A). In the dark, however, actin organization mainly appeared surrounding the amyloplasts both in wild-type and *rmd-2* endodermal cells (Fig. 4B). Moreover, the amyloplasts were predominantly located at the base of the cells (Fig. 4B). To further investigate these differences under light conditions, we extracted actin networks from actin cytoskeletal image data of light-grown wild type and *rmd-2* (Fig. 4, C and D) and analyzed network properties that provide measurements of the actin organization (Breuer et al., 2017). The results showed that the number of connected actin components was lower in *rmd-2* than in wild type (independent *t* test, *P* value: $P < 10^{-4}$), and the average edge capacity ("bundling") of actin in *rmd-2* shoot endodermal cells was higher than in the wild type ($P < 10^{-4}$; Fig. 4E), indicating that there are fewer AFs in the mutant. Furthermore, the average shortest path length and diameter of actin in *rmd-2* were bigger than in the wild type ($P < 10^{-7}$ and $P < 10^{-3}$, respectively; Fig. 4, E and F), suggesting that the actin-filament network in the mutant was less compact and nodes were in closer proximity to each other. These properties indicate that the wild-type actin network is more coherent and better suited for effective transport than that of the *rmd* mutants (Breuer et al., 2017).

RMD Is Diurnally Expressed and Regulated by Light Signaling Components

Because the RMD-mediated shoot negative gravitropic response is light-dependent, we next asked what the molecular link between light signaling, gravitropism, and RMD-mediated actin cytoskeleton organization might be. We first performed reverse transcription quantitative PCR (RT-qPCR) analysis of *RMD* and found that *RMD* transcript levels were substantially higher in light-grown than in etiolated seedlings (Supplemental Fig. S6A). Additionally, we sampled plants grown in the field every 4 h, and found that the abundance of the *RMD* transcript was oscillatory, with the highest level at 4 PM and lowest level at 4 AM (Supplemental Fig. S6B). This gene expression pattern was corroborated by data from the Rice Expression Profile Database (RDB, http://ricexpro.dna.affrc.go.jp/; Sato et al., 2011).

In Arabidopsis, hypocotyl growth orientation is controlled by phytochrome-mediated inhibition of negative gravitropism through PIFs (Lariguet and Fankhauser, 2004; Kim et al., 2011), which are nuclear proteins that integrate light and other signals, such as

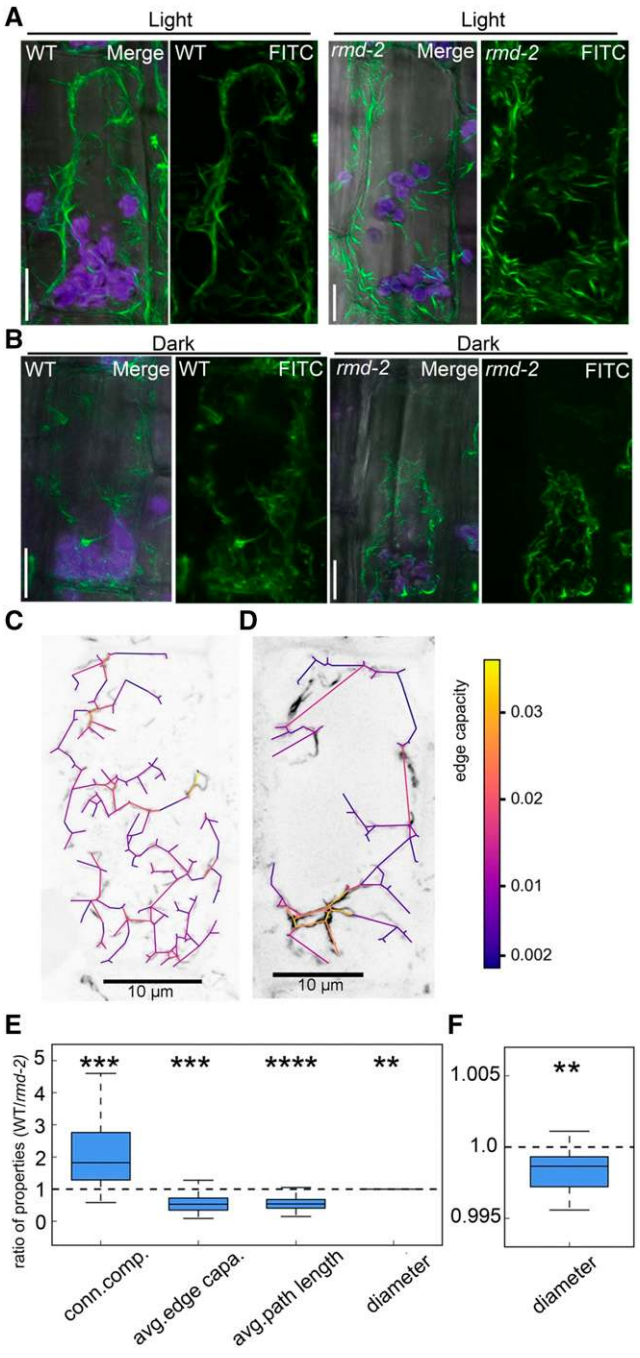

Figure 4. Disturbed actin cytoskeleton in shoot endodermis of light-grown *rmd* mutants. A and B, F-actin organization in shoot endodermal cells of light-grown (A) and etiolated (B) seedlings. Images were merged from Fluorescein isothiocyanate (FITC; green, F-actin) and Cy5 (cyan, amyloplasts) channels. Scale bars = 10 μm. C and D, Z-projected actin cytoskeleton with extracted network overlaid for (A) wild type ($n = 14$) and (B) *rmd-2* mutant ($n = 15$). The color bar represents edge-capacity values. E and F, Ratio of the indicated property values between wild type (WT; $n = 14$) and *rmd-2* ($n = 15$; E) and a magnified boxplot for diameter (F). Boxplots are shown with median (horizontal line), 25th and 75th percentiles (box edges), and 1.5× interquartile range (whiskers). Values are means ± SD. Student's *t* test: $^{**}P < 0.01$, $^{***}P < 0.001$, and $^{****}P < 0.0001$.

hormones and the circadian clock, to regulate gene expression (Leivar and Monte, 2014). To test whether *RMD* expression is controlled by PIF-related proteins, we first analyzed cis-regulatory elements of the *RMD* promoter (2 kb upstream of start codon), using the online analytical tool MatInspector (Cartharius et al., 2005), and identified three predicted PIF-binding elements (PBE: −1,576 bp, G-box: −849 bp and −639 bp; Fig. 5A). We therefore speculated that *RMD* could be regulated by PILs (PIF homologs in rice) through their binding to the *RMD* promoter. To test this hypothesis, and due to low level expression of one member, we cloned five *PIL* genes among the six members in the rice genome, including *OsPIL11*, *OsPIL13*, *OsPIL14*, *OsPIL15*, and *OsPIL16*, by RT-qPCR from rice cDNAs and placed each gene under the *CaMV35S* promoter. We also fused ~2 kb of the *RMD* promoter with the gene of firefly luciferase (LUC), and cotransformed *35S*::*OsPILs* with *pRMD*::LUC into *Nicotiana benthamiana*, using renilla luciferase (REN) as an internal control. Luciferase activity measurements showed that *LUC* expression was activated by OsPIL15, but repressed by OsPIL16 (Fig. 5B). Interestingly, OsPIL15 and OsPIL16 are homologous, and share a 33% protein sequence similarity (Supplemental Fig. S6C).

Because PIFs regulate downstream genes by binding to G-boxes and PBE-boxes in the promoter of the target genes (Kidokoro et al., 2009), we performed yeast one-hybrid (Y1H) and chromatin immunoprecipitation (ChIP)-qPCR assays to assess whether OsPIL15 and OsPIL16 could bind to these boxes within the *RMD* promoter. Y1H assays showed that OsPIL16 interacted

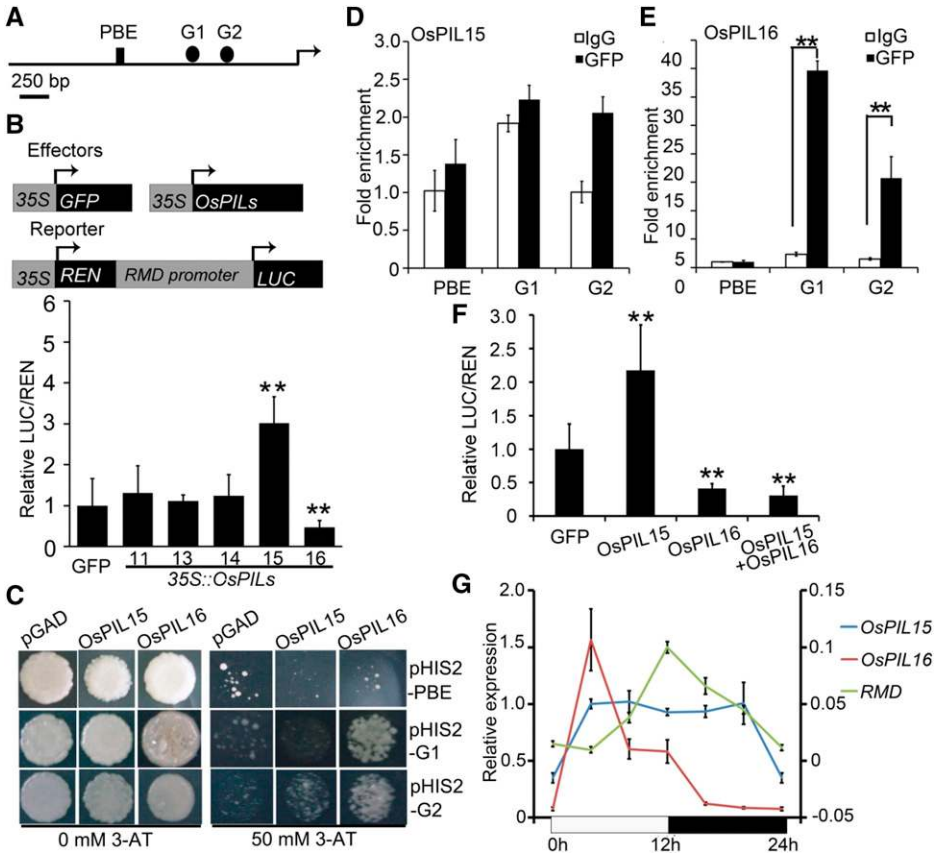

Figure 5. Regulation of *RMD* expression by OsPIL15 and OsPIL16. A, Cis-acting elements in the promoter of *RMD*. CACATG; G1 and G2, G-box, CACGTG. B, OsPIL15 activates *RMD* promoter activity and OsPIL16 inhibits *RMD* promoter activity in *N. benthamiana* leaf cells. Effectors are 35S::*OsPILs* and *35S*::*GFP* (control), and *pRMD*::*LUC* is the reporter. Renilla is the internal control whereby LUC activity was normalized to REN activity. Data were analyzed by conducting both *t* test and ANOVA. Data represent means ± SD ($n \geq 5$). $^{**}P < 0.01$. C, Y1H analysis. Interactions between OsPIL16 and G1 and G2, and between OsPIL15 and G2 in the promoter of *RMD*, are shown. D and E, ChIP-qPCR results showing binding of OsPIL15 (D) and OsPIL16 (E) to the *RMD* promoter fragments containing the PBE-box and G-box. Student's *t* test *P* values: $^{**}P < 0.01$. F, Co-expression of OsPIL15 and OsPIL16 inhibit *RMD* promoter activity in *N. benthamiana* leaf cells. Effectors are 35S::*OsPIL15*, 35S::*OsPIL16*, 35S::*OsPIL15*+*OsPIL16*, and *35S*::*GFP* (control), and *pRMD*::*LUC* is the reporter. Renilla is the internal control whereby LUC activity was normalized to REN activity. Data were analyzed by conducting both *t* test and ANOVA. Data represent means ± SD ($n \geq 5$). $^{**}P < 0.01$. G, RT-qPCR analysis of the diurnal expression pattern of *RMD* (right axis), *OsPIL15* (left axis), and *OsPIL16* (left axis) in growth chamber. Plants were placed in the 12-h/12-h light/dark cycle. Results are presented as means ± SD. Plants were placed in the 12-h/12-h light/dark cycle.

strongly with G1 and weakly with G2, while OsPIL15 interacted weakly with G2 (Fig. 5C). To investigate whether these PILs also bind to the *RMD* promoter in vivo, we generated rice transgenic lines expressing OsPIL15-GFP and OsPIL16-GFP (Supplemental Fig. S7, A and B). ChIP-qPCR assays using GFP antibodies on the nuclear protein–DNA complex extracted from the transgenic lines showed clear enrichment of the G1- and G2-boxes for OsPIL16, and slight enrichment of the G2-box for OsPIL15 (Fig. 5, D and E). Additional analysis of truncated *pRMD* constructs with the deletion of the above cis-elements showed that G1 and G2 were essential for OsPIL16's suppression of *RMD's* promoter activity, and that G2 was critical for OsPIL15 to activate *RMD's* promoter (Supplemental Fig. S7, C–E). Given that OsPIL15 activates and OsPIL16 represses *RMD* expression, we next assessed whether the *RMD* expression is induced or suppressed when both TFs are present. To do this, we coexpressed 35S-driven OsPIL15 and OsPIL16 and *pRMD*::LUC in *N. benthamiana* leaf cells and analyzed the promoter activity by dual-Luciferase (Dual-LUC) assay. These results clearly show that the *RMD* promoter activity was repressed (Fig. 5F), indicating that OsPIL16 has a stronger effect on *RMD* expression than OsPIL15.

As *RMD* exhibits diurnal expression, we also checked the expression of *OsPIL15* and *OsPIL16* using data from the RDB (http://ricexpro.dna.affrc.go.jp/). *OsPIL16* displayed an opposite expression pattern to that of *RMD*, whereas *OsPIL15* did not show significant diurnal expression, which we confirmed by RT-qPCR analyses (Fig. 5G). These data suggest that OsPIL15 might drive a basal expression of *RMD* during both day and night, but that OsPIL16 inhibits the *RMD* expression during the night when OsPIL16 is present. Due to the *RMD* promoter activity results, inverse expression relationship (Supplemental Fig. S6, A and D), and the strong interaction between *OsPIL16* and *RMD*, we chose to characterize the functional interactions of OsPIL16 and *RMD* in greater detail.

OsPIL16 Negatively Regulates *RMD* Gene Expression through Its bHLH Domain

OsPIL16 has two putative conserved motifs, an N-terminal PIL-motif possibly for the interaction with phytochromes and a C-terminal basic helix-loop-helix (bHLH) domain for DNA-binding (Nakamura et al., 2011; Supplemental Fig. S7F). To establish which region in OsPIL16 is responsible for repressing *RMD* expression, we fused each of these two motifs, or the full-length *OsPIL16* to the *binding domain* of GAL4, and performed transcriptional activation tests in yeast (Hao et al., 2010). The full-length OsPIL16, the PIL-containing OsPIL16-N, and the bHLH domain-containing OsPIL16-C conferred weak, strong, and no transcriptional activity in yeast, respectively (Supplemental Fig. S7G). Thus, we hypothesized that the bHLH domain of OsPIL16 might be responsible for repressing *RMD* transcriptional level. To test this hypothesis, we transiently coexpressed *OsPIL16* or *OsPIL16-C* with *pRMD*::*LUC* in *N. benthamiana*. Both constructs displayed reduced LUC activity compared with the control (Supplemental Fig. S7H). These data supported the conclusion that OsPIL16 represses *RMD* expression in rice through its C-terminal bHLH domain.

OsPIL16 Regulates Rice Growth and Shoot Gravitropism

If OsPIL16 is a negative regulator of *RMD* expression, overexpression (OE) of *OsPIL16* should mimic the *rmd* mutant phenotype to some degree. To this end, we generated transgenic rice plants expressing *35S*::*OsPIL16* and selected three independent lines that showed substantial reduction in *RMD* expression compared to the wild type (Supplemental Fig. S6, E and F). Similar to *rmd*, *OsPIL16* OE lines showed delayed shoot and root growth (Zhang et al., 2011; Li et al., 2014), and more transverse AFs in shoots (Supplemental Fig. S8, A–H). Quantification of the fluorescence intensity of the AlexaFluor488-phalloidin-labeled actin showed slightly weaker fluorescence signals in *OsPIL16*-OE lines than wild type in light, but not much difference in dark-grown seedlings (Supplemental Fig. S8, D and H), suggesting that OsPIL16 regulates actin cytoskeleton abundance via its repression of *RMD* in light.

We next checked whether *OsPIL16*-OE transgenic lines displayed an aberrant gravitropic response. The light-grown *OsPIL16*-OE transgenic lines displayed a reduced level of gravitropic response compared with wild type (Fig. 6, A and B), but this defect was less pronounced in etiolated seedlings (Fig. 6, C and D). Ten minutes after the light-grown seedlings were turned upside down, a large proportion of amyloplasts still remained in the middle of the shoot endodermal cells in *OsPIL16*-OE lines, which was in stark contrast to the wild type (Fig. 6, E, G, and H). However, most amyloplasts in the *OsPIL16*-OE lines finally reached the base of the cells in 20 min (Fig. 6, E, G, and H). Again, amyloplast sedimentation occurred at the same pace in etiolated wild-type and *OsPIL16*-OE seedlings (Fig. 6, F, G, and I). Together these results revealed striking similarities in phenotypic behavior of the *OsPIL16*-OE lines and the *rmd* mutant, providing strong evidence that *RMD* is negatively regulated by the light signaling component OsPIL16 and that this regulation is important for gravisensing in light-grown rice plants.

DISCUSSION

Shoot negative gravitropism is essential for plant architecture and yield (Li et al., 2007; Wu et al., 2013; Zhang et al., 2018). Seedling establishment is exquisitely sensitive to environmental cues and, after emergence from the soil, it is especially affected by the

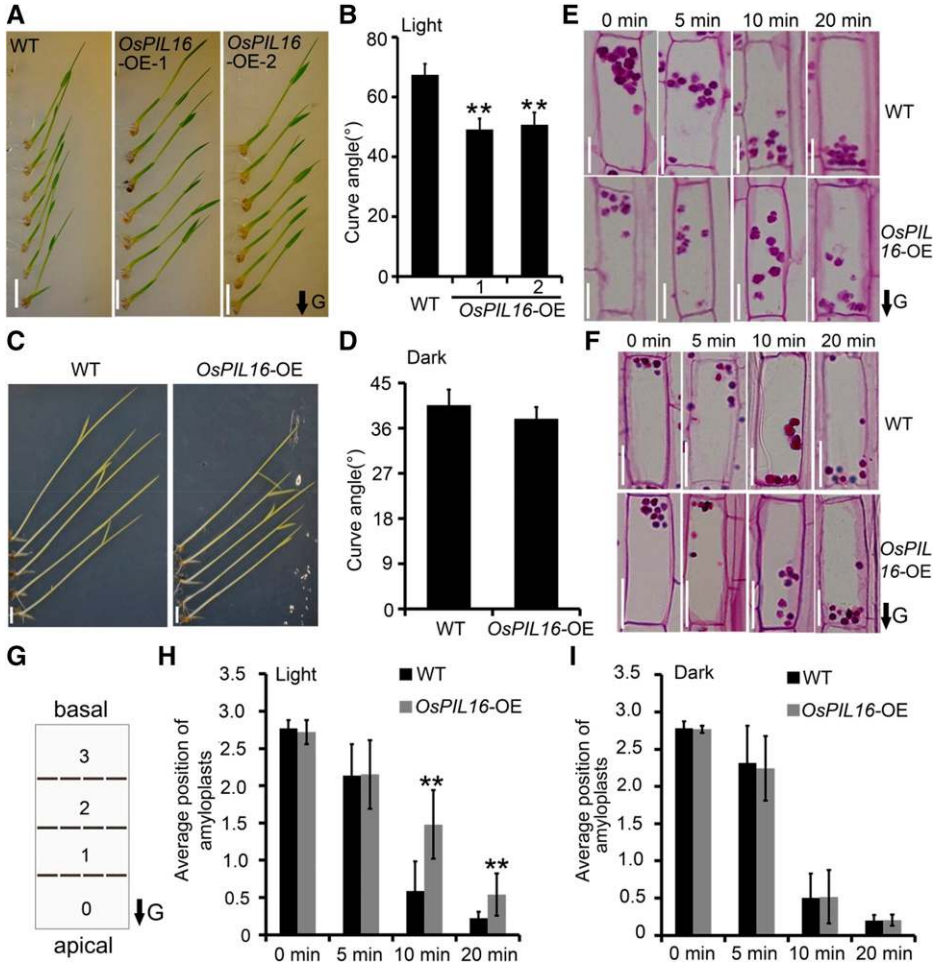

Figure 6. Analysis of gravitropism in *OsPIL16* OE lines. A, Five-days–old light-grown seedlings of wild type (WT) and *OsPIL16* OE lines 72 h after seedlings were turned 90°. Scale bars = 1 cm. Arrow indicates direction of gravity. B, Measurement of the angle of curves in shoots after gravistimulation. Data were analyzed by conducting both *t* test and ANOVA. Values are means ± SD. $n = 14$. $^{**}P < 0.01$. C, Five-d–old etiolated wild type and *OsPIL16*-OE 72 h after gravistimulation. Scale bars = 1 cm. D, Measurement of the angle of curves in etiolated wild type ($n = 13$) and *OsPIL16*-OE ($n = 13$) seedlings 72 h after gravistimulation. Values are means ± SD. E and F, Comparison of the kinetics of amyloplasts sedimentation in shoot endodermal cells in light-grown (E) and etiolated (F) wild type and *OsPIL16*-OE. Scale bars = 20 μm. Arrow indicates gravity direction. G, Schematic position of amyloplasts in endodermal cells. Each cell is divided into four equal segments numbered 0 to 3. Amyloplasts moved from basal to apical side after seedlings were inverted and their positions were scored. Arrow indicates direction of gravity. H, Average position of amyloplasts in light-grown wild type ($n = 84$ from four shoots) and *OsPIL16*-OE ($n = 84$ from four shoots) at different time points after seedlings were reoriented. Values (defined in G) are means ± SD. Student's *t* test: $^{**}P < 0.01$. I, Average position of amyloplasts in etiolated wild type ($n = 78$ from four shoots) and *OsPIL16*-OE ($n = 74$ from four shoots) at different time points after seedlings were reoriented. Values (defined in G) are means ± SD.

balance between the light/dark cycle and gravity (Gommers and Monte, 2018). In this work, we outline a mechanism for how plant shoots regulate their actin cytoskeleton to respond to gravitropic changes during the day to optimize seedling development.

AFs have long been suggested to be involved in shoot gravitropism through their ability to modulate amyloplast movement, but conflicting results have been reported (Yamamoto and Kiss, 2002; Hou et al., 2003; Palmieri and Kiss, 2005). Nevertheless, recent studies have indicated that AFs may act as tension sensors in the cell (Okamoto et al., 2015). In this study, we show that RMD is required for the organization of AFs, which impacts amyloplast behavior in shoot endodermal cells. RMD thus promotes negative gravitropism in rice shoots. Notably, even though *rmd* shoot endodermal and root columella cells had an impaired actin cytoskeleton, the amyloplasts sedimented faster in the columella cells and slower in the endodermal cells as compared to the control (Huang et al., 2018; Fig. 2). Hence, depending on the cellular context, RMD contributes differently to the gravitropic outputs. We speculate that this difference may be caused by the weak and ring-like F-actin surrounding amyloplasts in

root columella cells, but more abundant actin arrays in the shoot endodermal cells (Fig. 4). Indeed, previous studies showed that LatB-induced disruption of the actin cytoskeleton limited amyloplast dynamics in shoot endodermal cells, but induced settlement in root columella cells (Palmieri and Kiss, 2005). This again indicates a distinct role of F-actin in amyloplast dynamics during the gravitropic response in roots and shoots. The organ-specific gravitropic responses therefore suggest that the molecular mechanisms of gravitropic response vary between plant above- and below-ground organs. Furthermore, it is also plausible that vacuoles in shoot endodermal cells function as negative regulators of amyloplast sedimentation in shoot endodermal cells (Saito et al., 2005).

Interestingly, RMD only modulates shoot negative gravisensing in light-grown seedlings, linking the function of RMD to light signaling. Several studies have investigated the relationship between AFs and light, which is perhaps best described in the context of chloroplast movement under different light conditions (Wada and Kong, 2018). We hypothesize that, in light-grown plants, RMD promotes actin organization to support amyloplast distribution and as a result, gravisensing. This hypothesis agrees well with the localization of RMD to the amyloplast in the endodermis (Fig. 7). Similarly, E3 ligase protein SGR9 also localized on the surface of amyloplasts in the endodermis and positively modulated gravity sensing in Arabidopsis shoots (Nakamura et al., 2011). We therefore speculate that there is a possible link between RMD and protein-turnover components, such as E3 ligases; however, this remains to be elucidated. We previously presented in vitro biochemical data that RMD promotes AF formation and bundling (Zhang et al., 2011), and revealed the localization of RMD on chloroplast surface (via the phosphatase and tensin domain) in leaf cells (Zhang et al., 2011) and on the surface of statoliths in root

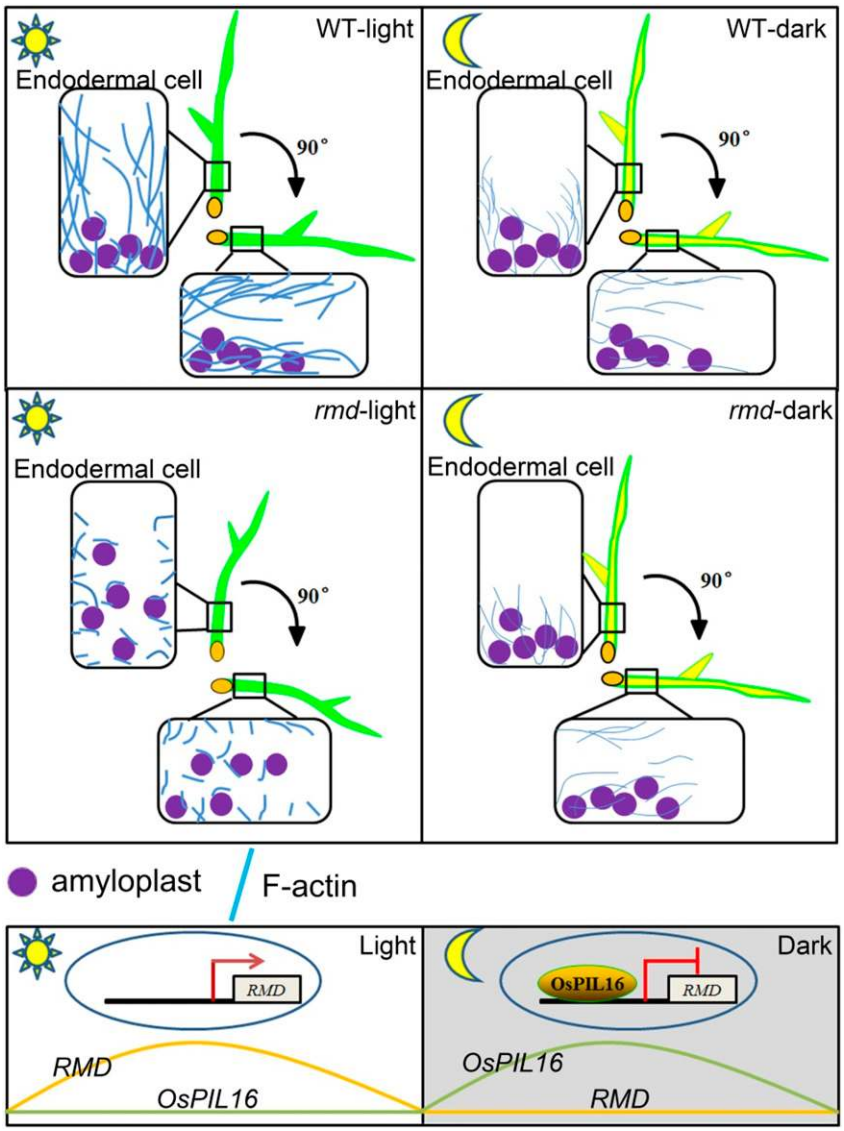

Figure 7. Schematic model for RMD function in light-mediated shoot negative gravitropism. In the dark and in the absence of phytochrome activity, OsPIL16 accumulates in the nucleus and inhibits *RMD* expression, changing actin organization in the endodermis to allow shoot negative gravitropism in etiolated seedlings. Upon exposure to light, the level of OsPIL16 is reduced, which allows expression of *RMD* and subsequent RMD-induced reorganization of the actin cytoskeleton that facilitates amyloplast dynamics in endodermal cells. In the absence of RMD, the endodermis fails to rearrange the actin organization, which reduces amyloplast sedimentation and consequently leads to abnormal shoot gravisensing in the light. WT, wild type.

columella cells (Huang et al., 2018). In this context, we postulate that RMD is anchored to amyloplasts via its phosphatase and tensin domain and that the formin domains of RMD orchestrate changes in AF organization in shoot endodermal cells.

In Arabidopsis, the light-mediated negative gravitropism of hypocotyls is inhibited by phytochromes through PIFs (Kim et al., 2011). However, the molecular mechanism and downstream components involved in this process are still not clear. In rice, Phytochrome A is important for the light-modulated root gravitropic response (Takano et al., 2001), indicating that gravisensing may also be modulated by light in rice shoots and that this phytochrome-mediated modulation of gravitropic response may be conserved in plants. Here, we provide evidence that the *RMD* gene is a direct target of the phytochrome interacting factor-like proteins OsPIL15 and OsPIL16, which regulate the expression of *RMD* during the diurnal cycle in rice. Specifically, OsPIL15 may maintain a "basal level" of *RMD* expression throughout the diurnal cycle as this TF is continuously on. By contrast, *OsPIL16* is only expressed during the night and strongly represses *RMD* expression and thus orchestrates changes in the actin cytoskeleton. OsPIL16 binds to the G-box of the *RMD* promoter through its C-terminal bHLH domain. Notably, despite OsPIL16 being a repressor of *RMD* expression, the N-terminal PIL-motif in OsPIL16 is a transcriptional activator, indicating that OsPIL16 may act as an activator or repressor depending on the circumstance. Similarly, the N terminus of AtPIF7 acts as a transcriptional activator in Arabidopsis, whereas its C-terminal bHLH domain repressed *DREB1* expression under circadian control (Kidokoro et al., 2009). Transcriptional activation via PIFs was also demonstrated in Arabidopsis (Moon et al., 2008; Sakuraba et al., 2014), indicating that PIFs have dual functions possibly depending on the promoter context. Interestingly, our analysis of 112 actin-related genes in rice (Supplemental Table S1), including those that encode formin, myosin, and actin-depolymerizing factors, revealed that the expression of 23 of them are diurnally regulated and 17 out of these 23 genes contain G-boxes in their promoters (Supplemental Fig. S9, A and B). Among these genes, we selected five members and conducted expression pattern analysis by RT-qPCR. Our results showed that these five genes indeed exhibited diurnal regulation (Supplemental Fig. S10, A–E). In addition, transferring dark-grown seedlings into light conditions impacted the transcriptional level of these genes (Supplemental Fig. S10F). These data further substantiate a close connection between light signaling and the actin cytoskeleton. In Arabidopsis, PIF1 share 19% protein sequence similarity of OsPIL15 and 24% of OsPIL16, required for photomorphogenesis and chlorophyll synthesis (Shen et al., 2005; Soy et al., 2014), but it is not clear whether Arabidopsis PIF1 plays a role in gravitropism and actin cytoskeleton patterning.

Based on our data, we propose a model in which rice shoot negative gravitropism is connected to light signaling via AFs (Fig. 7). In the dark, OsPIL16 accumulates and acts as a transcriptional repressor of *RMD*, and perhaps other actin-related genes, to change the organization of the actin cytoskeleton. When exposed to light, the level of OsPIL16 is possibly reduced, at least judging from transcript abundance, and *RMD* is consequently increased to modulate actin organization. As a result, amyloplast localization and movement are properly controlled in endodermal cells. In the absence of RMD, or when OsPIL16 is overexpressed, and thus *RMD* repressed, the actin cytoskeleton organization changes in light, which leads to aberrant amyloplast localization and movement, and abnormal shoot gravisensing (Fig. 7). In summary, our study has uncovered a mechanism underlying the intersection of light perception and gravitropism in plants.

MATERIALS AND METHODS

Plant Growth

All rice (*Oryza sativa*) plants are in the 9522 background (ssp. *japonica*). The two alleles, *rmd-1* and *rmd-2*, were generated by ^{60}Coray treatment from 9522. *rmd-1* contains a T-to-C transition and a four-nucleotide (AAGG) deletion in the 11th exon, leading to premature termination at the 1,465th amino acid. *rmd-2* has a four-nucleotide (ATGG) deletion in the 4th exon, leading to premature terminations at the 392nd amino acid. Rice seedlings were grown on 1% (w/v) agar in growth chambers under a 12-h light/12-h dark cycle at 30°C light/28°C dark. *Nicotiana benthamiana* plants were grown in growth chambers at 23°C with a 16-h light/8-h dark cycle. Seedlings were photographed using a model no. E995 Digital Camera (Nikon).

Generation of Rice Transgenic Lines

The *rmd-1* and *rmd-2* mutants, and *pLex*::*RMD-RFP* and *ProRMD*::*RMD-GFP* transgenic lines used in this study were described in Zhang et al. (2011), Li et al. (2014), and Huang et al. (2018). *ProOsPIN1b*::*OsPIN1b-YFP* was created by inserting the *PIN1b* cDNA (*AK102343*) into *Spe*I and *Sma*I sites of pA7-YFP, followed by the insertion of *OsPIN1b-YFP* into *Sma*I and *Eco*RI sites of *pCAMBIA1301*. The ~3-kb promoter of *OsPIN1b* was cloned from BAC *OSJNBa0055K09* and inserted into *Bst*EII and *Eco*RV sites of *pCAMBIA1301-OsPIN1b-YFP*. *ProOsPIN1b*::*OsPIN1b-YFP*/*rmd-2* was obtained by crossing *ProOsPIN1b*::*OsPIN1b-YFP*/*9522* with *rmd-2*. The *OsPIL15*-overexpressing construct was created by inserting the 1,911-bp *OsPIL16* cDNA into the *Nco*I and *Bgl*II sites of *pCAMBIA1301*. The *OsPIL16*-overexpressing construct was created by inserting the 1,512-bp *OsPIL16* cDNA into the *Bgl*II and *Spe*I sites of *pCAMBIA1301*. The final constructs were transformed into wild-type rice callus by *Agrobacterium tumefaciens*-mediated transformation. Primers used to create *pCAMBIA1301-OsPIN1b-YFP*-and *OsPIL16*-overexpressing lines are listed in Supplemental Table S2.

Gravitropism Assay

After sterilizing with 70% (v/v) ethanol for 2 min and then washing five times with double-distilled water, rice seeds were placed on three layers of filter paper in plates containing half-strength liquid MS at 28°C. Two-d–old seedlings without true leaf outgrowth, or a 5-d–old seedling with one true leaf, were used for quantification. At these stages, the gravitropic set-point angle (GSA) was at the base of the seedlings (Fig. 2A). As shown in Figure 1A, except for S-shape and twisted *rmd* mutants, the base of *rmd* bending seedlings was straight, and we thus selected this type of mutant for the analysis. The seedlings were transferred to a new agar plate and kept for 3 h of vertical growth before being turned 90° and grown under dim and nondirectional light. The gravitropic curvature was determined by measuring the angle of the reoriented shoots using the software ImageJ (National Institutes of Health).

Histochemical Analysis

For histochemical analysis, 5-d–old seedlings grown in the soil were selected. Tissue was cut close by the GSA and quickly fixed in 10% (v/v) formaldehyde, 5% (v/v) acetic acid, and 50% (v/v) ethanol in vertical position for 30 min in 0.2-mL tubes under vacuum. After fixation, samples were dehydrated in 30%, 50%, 70%, 80%, 95%, 100%, and 100% (v/v) ethanol for 30 min at each concentration. Samples were infiltrated and embedded in Technovit 7100 resin embedding kit (Heraeus Kulzer). Infiltration solution was prepared by dissolving 1 g of Hardener I into 100 mL of Basic resin. Then samples were pre-infiltrated in a mixed solution of 100% ethanol and infiltration solution (v/v = 1:1) for 2 h. After this, samples were transferred into infiltration solution and kept overnight. The embedding solution was prepared just before use, by mixing Hardener II and the infiltration solution at a ratio of 1:15. Samples in the embedding solution were kept at 37°C until solidifying. Sections (5 μm) were made using a semi-thin microtome (Leica Microsystems), and stained with 0.5% (w/v) toluidine blue. The periodic acid-Schiff kit (Sigma-Aldrich) was used to stain amyloplasts for amyloplast sedimentation analysis (Wu et al., 2013). Photos were taken with an Ni-E Optical Microscope (Nikon). For each time point, the amyloplast positions in at least 70 endodermal cells were examined from four different shoots.

Pharmacological Treatments

LatB (10 mM; Sigma-Aldrich) and estradiol (50 mM; Sigma-Aldrich) were kept as stock solutions in dimethyl sulfoxide. The desired concentration of LatB and estradiol was obtained by diluting each chemical in water (Yamamoto and Kiss, 2002). After germination, seeds were put on top of the three layers of filter paper in a bottle containing half-stength liquid MS with LatB or estradiol, without being immersed into the liquid medium. Seedlings were photographed using a model no. E995 Digital Camera (Nikon).

F-Actin Staining

F-actin staining and fluorescence quantification was performed as described in Zhang et al. (2011) and Yang et al. (2011) with slight modification. Shoots were cut from ~5-d–old rice seedlings. Tissue was cut close to the GSA. Then samples were incubated for 1 h in PEM buffer (100 mM of Piperazine-1,4-bisethanesulfonic acid, 10 mM of EGTA, 5 mM of $MgSO_4$, and 0.3 M of mannitol at pH = 6.9) that contains 2% (v/v) glycerol (Sigma-Aldrich) and 6.6 μM of Alexa Fluor 488-phalloidin (Invitrogen), and then observed in 50% (v/v) glycerol (Sigma-Aldrich) with a model no. A1R Laser Scanning Confocal Microscope (Nikon). At least 10 cells from three different lines were examined.

Microscopic Analysis

Confocal microscopy was conducted with a model no. A1R Laser Scanning Confocal Microscope (Nikon). Fluorescence signals for GFP and amyloplast autofluorescence were detected with 500- to 510-nm and 640- to 700-nm settings respectively, with the excitation wavelength of 488 nm. Images were extracted with an NIS-Elements Viewer 4.20 (Nikon) and processed with the software Adobe Photoshop CS6 (Adobe).

Dual-LUC Assay

Dual-LUC assay was performed using *N. benthamiana* plants. With the exception of *OsPIL12*, all of the rice PILs (*OsPIL11*, *13*, *14*, *15*, and *16*) were successfully cloned. Effectors were constructed by cloning full-cDNAs of *OsPILs* into *Hin*dIII and *Xba*I sites of the pGreenII-0000 vector, under the control of *35S* promoter, and *35S::OsPIL16C* was constructed by inserting a 510-bp C-terminal sequence of *OsPIL16* into *Hin*dIII and *Eco*RI sites of the same vector. For co-expression of OsPIL15 and OsPIL16, the whole length of the *35S* promoter and *OsPIL15* were amplified and cloned into *Xba*I sites of the pGreenII-0000 vector. Reporters *pGreen-pRMD::LUC*, *pGreen-pRMDδI::LUC*, *pGreen-pRMDδII::LUC*, and *pGreen-pRMDδIII::LUC* were constructed by fusing firefly LUC with the truncated *RMD* promoters, followed by insertion of the final construct into *Hin*dIII and *Nco*I sites of the pGreenII-0800 vector. REN was the internal control.

Effectors and reporters were cotransformed into *Agrobacterium* (strain GV3101) with the helper plasmid pSoup-19. *Agrobacterium* was resuspended with MS medium (pH = 5.8) and adjusted to OD_{600} = 0.6 before MES (pH = 5.6, 10-μM final concentration) and acetosyringone (200-μM final concentration) were added. After incubation for ~3 h at room temperature, the *Agrobacterium* mixture (reporter: effector ratio at 2:8) was infiltrated into young *N. benthamiana* leaves with a 1-mL syringe. Plants were kept under weak light conditions for 48 h.

LUC and REN activities were tested using dual-LUC assay reagents (Promega) according to the manufacturer's instructions. LUC/REN values were measured in a Turner 20/20 Luminometer (Promega). At least five biological replicates were measured for each sample. The primer sequences used to perform Dual-LUC assay are listed in Supplemental Table S2.

Y1H Assay

Fragments of the *RMD* promoter that contain PBE-box (163 bp) or G-boxes (164 bp, 189 bp) were amplified and cloned into *Sac*I and *Sac*II sites of the pHIS2 vector (Clontech). Full-length cDNAs of *OsPIL15* and *OsPIL16* were amplified and inserted into *Nde*I and *Bam*HI sites of pGADT7 (Clontech). Yeast strain Y187 was used to perform Y1H. Y187 was incubated in a YPD medium (yeast extract 10 g/L, peptone 20 g/L, and dextrose 16 g/L medium) at 30°C overnight. Constructed pHIS2 and pGADT7 plasmids were prepared with cDNA, and cotransformed into yeast strain by incubating with 100 mM of DTT, 0.2 M of lithium acetate, and 40% (w/v) polyethylene glycol at 45°C for 30 min. Protein–DNA interactions among OsPIL15, OsPIL16, and various *RMD* promoter fragments were analyzed in SD/-Trp/-Leu/-His medium containing 0 mM or 50 mM of 3-amino-11, 2, 4-triazole. Primer sequences used in the Y1H assay are listed in Supplemental Table S2.

ChIP qPCR Assay

The ChIP assay was performed using a protocol described in Bowler et al. (2004). Two-week–old *35S::OsPIL15-GFP* or *35S::OsPIL16-GFP* transgenic seedlings were used to isolate chromatin. Seedlings (200 g) were cut into pieces in 50 mL of EB1 buffer (10 mM of Tris-HCl at pH = 8.0, 0.4 M of Suc, 0.1 mM of Phenylmethanesulfonyl fluoride, and 5 mM ofβ-Mercaptoethanol [β-ME]) containing 1% (v/v) formaldehyde and then kept under vacuum for 30 min, after which 0.125 M of Gly was added to stop cross-linking and samples were washed with water 8–10 times to eliminate elution buffer (EB1). Then, samples were ground in 30 mL of EB1 buffer without formaldehyde, and filtered at 2,880 g through four layers of Miracloth (EMD Millipore) for 20 min. After the supernatant was discarded, samples were resuspended in 1 mL of EB2 solution (10 mM of Tris-HCl at pH = 8.0, 0.25 M of Suc, 10 mM of $MgCl_2$, 1% [v/v] TritonX-100, 5 mM of β-ME, 0.1 mM of PMSF, and protease inhibitor), centrifuged at 20,000*g* for 5 min, and resuspended with 300 μL of EB3 (10 mM of Tris-HCl at pH = 8.0, 1.7 M of Suc, 2 mM of $MgCl_2$, 0.15% [v/v] TritonX-100, 5 mM of β-ME, 0.1 mM of PMSF, and protease inhibitor) before gentle transfer into a new tube containing EB3 solution in the same volume. Samples were centrifuged at 16,000*g* for 1 h and resuspended in 250 μL of nuclei lysis buffer (1% [w/v] SDS, 50 mM of Tris-HCl at pH = 8.0, 10 mM of EDTA, 0.1 mM of PMSF, and protease inhibitor), and then stored at −20°C. Chromatins that are 500 bp to 1 kb were obtained by sonication, after which the supernatants that contained complexes of nuclear protein and nucleic acid were collected.

For immunoprecipitation, firstly we added 900 μL of ChIP dilution buffer (16.7 mM of Tris-HCl at pH = 8.0, 1.2 mM of EDTA, 167 mM of NaCl, 1% [v/v] Triton X-100, 0.1 mM of PMSF, and protease inhibitor) into 100-μL complex to dilute SDS, then added 40 μL of Protein A/G agarose/salmon sperm DNA beads, shaken slightly at 4°C for 1 h. After collecting supernatants, we continued to add IgG and GFP antibody, and samples were incubated and agitated gently overnight at 4°C. Then we collected immunoprecipitate by adding protein A agarose beads and agitating gently for 1 h at 4°C. The immunoprecipitated protein–DNA complexes were eluted with 0.1 M of $NaHCO_3$ containing 1% (w/v) SDS. We reversed the cross-link by incubation at 65°C with 250 mM of NaCl. For extracting DNA, first we incubated samples with 20 μL of 1 M Tris-HCl at pH = 6.5, 10 μL of 0.5 M EDTA, and 1.5 μL of 14 mg/mL proteinase K at 45°C for 1 h. Then we obtained DNA by phenol/chloroform extraction and ethanol precipitation. For qPCR reactions, the recovered DNA was used as a template, with three biological replicates. The primers used in the ChIP-qPCR assay are listed in Supplemental Table S2.

Transcriptional Activity Detection in Yeast

For transcriptional activity assay in yeast, *OsPIL16*, *OsPIL16N*, and *OsPIL16C* were introduced into pGBKT7 by inserting full-length (the 330-bp N-terminal region or the 510-bp C-terminal region) *OsPIL16* into the restriction sites *Nde*I and *Eco*RI. Y1H assays were performed following the manufacturer's instructions (Clontech). Yeast strain AH109 was used to perform the assay. pGBKT7-OsPIL16, pGBKT7-OsPIL16N, pGBKT7-OsPIL16C, and pGBKT7 were transformed into yeast strain AH109 individually, just as mentioned in "Y1H Assay." To test the transcriptional activity conferred by OsPIL16 on the promoter, yeast colonies were kept at 28°C for 2–3 d in SD-Trp and SD-Trp-His medium. Primers used for Y1H constructs are listed in Supplemental Table S2.

Assays to Measure IAA Level and Polar Transport

Inside or outside shoot segments from 5-d–old seedlings were collected for quantification of endogenous free auxin. IAA levels were measured as described in Barbez et al. (2012) with slight modification. Materials were grinded with 1 mL of cold P buffer (50 mM, pH = 7.0) and free IAA was extracted with methanol. Analysis was done by gas chromatography–mass spectrometry. Data presented are the means of three independent lots with 30–50 seedlings in each lot.

IAA polar transport was measured according to the method described in Lin et al. (2009). One-d–old coleoptiles were kept in darkness in MS liquid medium containing phytogel and 0.1 μM of ^{3}H-labeled IAA (American Radiolabeled Chemicals) at 28°C room temperature. N-1-naphthylphthalamic acid was used as a negative control to block IAA transport; shootward IAA transport was also used as a negative control. After incubation for ~3 h, 5 mm of nonsubmerged coleoptiles were excised and transferred into 2 mL of scintillation liquid (0.03% [w/v] 1,4-bis[5-phenyloxazol-2-yl] benzene, 0.3% [w/v] 2,5-diphenyloxazole, 80% [w/v] methylbenzene, 20% [v/v] glycol ether), then incubated for 18 h, before radioactivity was measured by a liquid scintillation counter (LS650; Beckman).

RNA Extraction and mRNA Expression Analysis

For RT-qPCR analysis, total RNA was isolated with the TRIZOL Reagent (Invitrogen). cDNA was synthesized from 4 μg of total RNA with M-MLV reverse transcriptase (Primescript RT Reagent Kit; Takara). RT-qPCR was performed using CFX384 (Bio-Rad) with the SYBR FAST qPCR Master Mix (KAPA Bio). Rice *Ubiquitin* mRNA was used as an internal control. For RT-qPCR assays, cDNA was denatured at 95°C for 10 min, followed by 45 cycles of 10^{-s} 95°C, 15^{-s} 58°C, and 15^{-s} 72°C. All results were presented as the means of three biological replicates. Primers used for gene expression analysis are listed in Supplemental Table S2.

Phylogenetic Analysis and Expression Profiling

Full-length amino acid sequences of PIL family members in Arabidopsis and rice were used to construct the phylogenetic tree using the software ClustalW (https://www.genome.jp/tools-bin/clustalw) for amino acid alignment, and the software MEGA 6.0 (https://www.megasoftware.net/) and the neighbor-joining tree method with a Poisson model, partial deletion, and bootstrap (1,000 replicates) were used for tree construction (Hall, 2013).

Accession numbers used to construct phylogenetic trees are as follows: *AtPIF1*, AT2G20180; *ATPIL1*, AT2G46970; *AtPIF3*, AT1G09530; *AtPIF4*, AT2G43010; *AtPIF5*, AT3G59060; *AtPIF6*, AT3G62090; *AtPIF7*, AT5G61270; *AtPIF8*, AT4G00050; *OsPIL11*, Os12g0610200; *OsPIL12*, Os03g0639300; *OsPIL13*, Os03g0782500; *OsPIL14*, Os07g0143200; *OsPIL15*, Os01g0286100; and *OsPIL16*, Os05g0139100.

The GENESIS software platform (http://genesis-sim.org/) was used to profile gene expression (Sturn et al., 2002). Gene expression data were downloaded from the RDB (http://ricexpro.dna.affrc.go.jp/; Sato et al., 2011). An expression image was calculated and imported in the software after loading the data. We set the upper maximum value as 1.0, and lower maximum value as −1.0. The operating procedure is based on the GENESIS manual written by Sturn et al. (2002).

Quantitative Analysis of the Actin Cytoskeleton

Actin networks extracted from images were analyzed using the automated extraction pipeline described in Breuer et al. (2017). Shoots of ~5-d–old rice seedlings were selected, from which we cut away the epidermis layers. Endodermal cell layers were quickly transformed into and were kept vertically in PEM buffer that contains 2% (v/v) glycerol (Sigma-Aldrich) and 6.6 μM of Alexa Fluor 488-phalloidin (Invitrogen). Samples were incubated for 1 h. After that, we imaged the actin cytoskeleton in wild-type and *rmd-2* endodermal rice cells as described in the "F-Actin Staining" and "Microscopic Analysis" sections and processed the images using a Fiji pipeline (National Institutes of Health) by correcting for bleaching, uneven illuminated background, and drifting of cells (Schindelin et al., 2012). Because the images consisted of multiple slices that were taken at different focal distances, we used the maximum intensity Z-projection to combine them into a composite image.

Afterward, we selected the region of interest and enhanced tube-like structures, before binarizing the image with an adaptive threshold and skeletonizing the binarized cytoskeleton, i.e. representing it as a one-pixel–wide skeleton. From the resulting skeleton, we identified nodes (end-points and crossings) that were connected with an edge if they were directly connected. The resulting networks were finally weighted according to their average AF thickness and selected network-based properties were calculated.

Aside from the properties analyzed in Breuer et al. (2017), e.g. the number of connected components, average edge capacity, and average shortest path length, we also computed the diameter of the extracted networks and normalized the extracted values by the expected diameter following Moore's bound $D_{exp} = \log_{\Delta} n$, where Δ is the maximum degree and n is the largest number of edges. An independent two-sample t test was used to compare the calculated properties of wild-type and *rmd-2* mutant networks. We used 14 replicates for the wild type and 15 replicates for the *rmd-2* mutant. From each image we extracted the actin cytoskeleton network and calculated the above-mentioned properties.

Statistical Analyses

Statistical analyses were performed with the software SPSS 22.0 (IBM). For the two groups' comparison, we used one-tailed Student's t test. For multiple comparisons, both the Student's t test and ANOVA followed by the posthoc test least-significant difference method were performed, which are mentioned in the figure legends. Values are means ± SD. At least three biological replicates are shown (P values: one asterisk shows significance at $P < 0.05$, two asterisks show significance at $P < 0.01$, three asterisks show significance at $P < 0.001$, and four asterisks show significance at $P < 0.0001$).

Accession Numbers

Sequence data used in this article can be found from the National Center for Biotechnology Information database under the following accession numbers: *OsPIL15*, Os01g0286100; *OsPIL16*, Os05g0139100; *Osmyosin-1*, LOC_Os07g37560; *OsOpaque10*, LOC_Os03g49630; *OsARP8*, LOC_Os04g57210; *OsFH3*, LOC_Os10g02980; *OsFH5*, LOC_Os07g40510; *OsFH6*, LOC_Os08g17820; *OsFH13*, LOC_Os07g39920; *OsFH15*, LOC_Os09g34180; *OsADF1*: LOC_Os02g44470; *OsADF2*: LOC_Os03g56790; *OsADF3*: LOC_Os03g60580; and *OsADF11*: LOC_Os12g43340.

Supplemental Data

The following supplemental materials are available.

Supplemental Figure S1. Growth direction of 4-d–old light-grown wild-type and rmd-2 shoots at intervals at 20°.

Supplemental Figure S2. Complementation of *rmd* by the estradiol-inducible *RMD* transgene and localization of OsPIN1b-YFP.

Supplemental Figure S3. Shoot negative gravitropism assay 2 d after germination.

Supplemental Figure S4. Distribution of amyloplasts wild-type and *rmd* seedlings.

Supplemental Figure S5. The effect of LatB on shoot gravitropism in plants.

Supplemental Figure S6. Expression patterns of *RMD* and *OsPIL16*, and phylogenetic analysis of PIL family proteins.

Supplemental Figure S7. OsPIL15 and OsPIL16 directly regulate *RMD* expression.

Supplemental Figure S8. OE lines of *OsPIL16* exhibit aberrant development and actin organization.

Supplemental Figure S9. Expression of rice genes putatively involved in actin cytoskeleton regulation and their promoter analysis.

Supplemental Figure S10. Diurnal expression patterns and light-induced expression of selected actin-related genes.

Supplemental Table S1. Accession number, annotation, and expression data downloaded from the Rice Expression Profile Database (RiceXPro) of 112 actin-related genes.

Supplemental Table S2. Sequences of primers used in this study.

ACKNOWLEDGMENTS

The authors thank Mingjiao Chen and Zhijing Luo (Shanghai Jiao Tong University) for performing rice cultivation, Gwen Mayo (Adelaide Microscopy) for assistance in the microscopy work, Dan Peet (the University of Adelaide) for providing the LUC luminometer, and Hongquan Yang for providing pGreenII-0000 and pGreenII-0800 vectors.

Received April 25, 2019; accepted July 30, 2019; published August 15, 2019.

LITERATURE CITED

Baluška F, Jasik J, Edelmann HG, Salajová T, Volkmann D (2001) Latrunculin B-induced plant dwarfism: Plant cell elongation is F-actin-dependent. Dev Biol **231:** 113–124

Barbez E, Kubeš M, Rolčík J, Béziat C, Pěnčík A, Wang B, Rosquete MR, Zhu J, Dobrev PI, Lee Y, et al (2012) A novel putative auxin carrier family regulates intracellular auxin homeostasis in plants. Nature **485:** 119–122

Behringer FJ, Lomax TL (1999) Genetic analysis of the roles of phytochromes A and B1 in the reversed gravitropic response of the *lz-2* tomato mutant. Plant Cell Environ **22:** 551–558

Blancaflor EB, Masson PH (2003) Plant gravitropism. Unraveling the ups and downs of a complex process. Plant Physiol **133:** 1677–1690

Bowler C, Benvenuto G, Laflamme P, Molino D, Probst AV, Tariq M, Paszkowski J (2004) Chromatin techniques for plant cells. Plant J **39:** 776–789

Breuer D, Nowak J, Ivakov A, Somssich M, Persson S, Nikoloski Z (2017) System-wide organization of actin cytoskeleton determines organelle transport in hypocotyl plant cells. Proc Natl Acad Sci USA **114:** E5741–E5749

Cartharius K, Frech K, Grote K, Klocke B, Haltmeier M, Klingenhoff A, Frisch M, Bayerlein M, Werner T (2005) MatInspector and beyond: Promoter analysis based on transcription factor binding sites. Bioinformatics **21:** 2933–2942

Ding Z, Galván-Ampudia CS, Demarsy E, Łangowski Ł, Kleine-Vehn J, Fan Y, Morita MT, Tasaka M, Fankhauser C, Offringa R, et al (2011) Light-mediated polarization of the PIN3 auxin transporter for the phototropic response in *Arabidopsis*. Nat Cell Biol **13:** 447–452

Dong Z, Jiang C, Chen X, Zhang T, Ding L, Song W, Luo H, Lai J, Chen H, Liu R, et al (2013) Maize LAZY1 mediates shoot gravitropism and inflorescence development through regulating auxin transport, auxin signaling, and light response. Plant Physiol **163:** 1306–1322

Fukaki H, Fujisawa H, Tasaka M (1996) *SGR1, SGR2, SGR3*: Novel genetic loci involved in shoot gravitropism in *Arabidopsis thaliana*. Plant Physiol **110:** 945–955

Fukaki H, Wysocka-Diller J, Kato T, Fujisawa H, Benfey PN, Tasaka M (1998) Genetic evidence that the endodermis is essential for shoot gravitropism in *Arabidopsis thaliana*. Plant J **14:** 425–430

Gaiser JC, Lomax TL (1993) The altered gravitropic response of the *lazy-2* mutant of tomato is phytochrome regulated. Plant Physiol **102:** 339–344

Gommers CMM, Monte E (2018) Seedling establishment: A dimmer switch-regulated process between dark and light signaling. Plant Physiol **176:** 1061–1074

Hall BG (2013) Building phylogenetic trees from molecular data with MEGA. Mol Biol Evol **30:** 1229–1235

Hao YJ, Song QX, Chen HW, Zou HF, Wei W, Kang XS, Ma B, Zhang WK, Zhang JS, Chen SY (2010) Plant NAC-type transcription factor proteins contain a NARD domain for repression of transcriptional activation. Planta **232:** 1033–1043

Hobbie L, Estelle M (1995) The *axr4* auxin-resistant mutants of *Arabidopsis thaliana* define a gene important for root gravitropism and lateral root initiation. Plant J **7:** 211–220

Hou G, Mohamalawari DR, Blancaflor EB (2003) Enhanced gravitropism of roots with a disrupted cap actin cytoskeleton. Plant Physiol **131:** 1360–1373

Huang G, Liang W, Sturrock CJ, Pandey BK, Giri J, Mairhofer S, Wang D, Muller L, Tan H, York LM, et al (2018) Rice actin binding protein RMD controls crown root angle in response to external phosphate. Nat Commun **9:** 2346

Kidokoro S, Maruyama K, Nakashima K, Imura Y, Narusaka Y, Shinwari ZK, Osakabe Y, Fujita Y, Mizoi J, Shinozaki K, et al (2009) The phytochrome-interacting factor PIF7 negatively regulates *DREB1* expression under circadian control in Arabidopsis. Plant Physiol **151:** 2046–2057

Kim K, Shin J, Lee SH, Kweon HS, Maloof JN, Choi G (2011) Phytochromes inhibit hypocotyl negative gravitropism by regulating the development of endodermal amyloplasts through phytochrome-interacting factors. Proc Natl Acad Sci USA **108:** 1729–1734

Kiss JZ (2000) Mechanisms of the early phases of plant gravitropism. CRC Crit Rev Plant Sci **19:** 551–573

Lariguet P, Fankhauser C (2004) Hypocotyl growth orientation in blue light is determined by phytochrome A inhibition of gravitropism and phototropin promotion of phototropism. Plant J **40:** 826–834

Leivar P, Monte E (2014) PIFs: Systems integrators in plant development. Plant Cell **26:** 56–78

Li G, Liang W, Zhang X, Ren H, Hu J, Bennett MJ, Zhang D (2014) Rice actin-binding protein RMD is a key link in the auxin-actin regulatory loop that controls cell growth. Proc Natl Acad Sci USA **111:** 10377–10382

Li G, Yang X, Zhang X, Song Y, Liang W, Zhang D (2018) Rice morphology determinant-mediated actin filament organization contributes to pollen tube growth. Plant Physiol **177:** 255–270

Li P, Wang Y, Qian Q, Fu Z, Wang M, Zeng D, Li B, Wang X, Li J (2007) *LAZY1* controls rice shoot gravitropism through regulating polar auxin transport. Cell Res **17:** 402–410

Lin H, Wang R, Qian Q, Yan M, Meng X, Fu Z, Yan C, Jiang B, Su Z, Li J, et al (2009) DWARF27, an iron-containing protein required for the biosynthesis of strigolactones, regulates rice tiller bud outgrowth. Plant Cell **21:** 1512–1525

Mirza JI, Olsen GM, Iversen TH, Maher E (1984) The growth and gravitropic responses of wild-type and auxin-resistant mutants of *Arabidopsis thaliana*. Physiol Plant **60:** 516–522

Moon J, Zhu L, Shen H, Huq E (2008) PIF1 directly and indirectly regulates chlorophyll biosynthesis to optimize the greening process in *Arabidopsis*. Proc Natl Acad Sci USA **105:** 9433–9438

Morita MT (2010) Directional gravity sensing in gravitropism. Annu Rev Plant Biol **61:** 705–720

Morita MT, Sakaguchi K, Kiyose S, Taira K, Kato T, Nakamura M, Tasaka M (2006) A C2H2-type zinc finger protein, SGR5, is involved in early events of gravitropism in Arabidopsis inflorescence stems. Plant J **47:** 619–628

Nakamura M, Toyota M, Tasaka M, Morita MT (2011) An *Arabidopsis* E3 ligase, SHOOT GRAVITROPISM9, modulates the interaction between statoliths and F-actin in gravity sensing. Plant Cell **23:** 1830–1848

Okamoto K, Ueda H, Shimada T, Tamura K, Kato T, Tasaka M, Morita MT, Hara-Nishimura I (2015) Regulation of organ straightening and plant posture by an actin–myosin XI cytoskeleton. Nat Plants **1:** 15031

Palmieri M, Kiss JZ (2005) Disruption of the F-actin cytoskeleton limits statolith movement in *Arabidopsis* hypocotyls. J Exp Bot **56:** 2539–2550

Poppe C, Hangarter RP, Sharrock RA, Nagy F, Schäfer E (1996) The light-induced reduction of the gravitropic growth-orientation of seedlings of *Arabidopsis thaliana* (L.) Heynh. is a photomorphogenic response mediated synergistically by the far-red-absorbing forms of phytochromes A and B. Planta **199:** 511–514

Robson PR, Smith H (1996) Genetic and transgenic evidence that phytochromes A and B act to modulate the gravitropic orientation of *Arabidopsis thaliana* hypocotyls. Plant Physiol **110:** 211–216

Saito C, Morita MT, Kato T, Tasaka M (2005) Amyloplasts and vacuolar membrane dynamics in the living graviperceptive cell of the Arabidopsis inflorescence stem. Plant Cell **17:** 548–558

Sakuraba Y, Jeong J, Kang MY, Kim J, Paek NC, Choi G (2014) Phytochrome-interacting transcription factors PIF4 and PIF5 induce leaf senescence in *Arabidopsis*. Nat Commun **5:** 4636

Sato Y, Antonio BA, Namiki N, Takehisa H, Minami H, Kamatsuki K, Sugimoto K, Shimizu Y, Hirochika H, Nagamura Y (2011) RiceXPro: A platform for monitoring gene expression in *japonica* rice grown under natural field conditions. Nucleic Acids Res **39:** D1141–D1148

Schindelin J, Arganda-Carreras I, Frise E, Kaynig V, Longair M, Pietzsch T, Preibisch S, Rueden C, Saalfeld S, Schmid B, et al (2012) Fiji: An open-source platform for biological-image analysis. Nat Methods **9:** 676–682

Shen H, Moon J, Huq E (2005) PIF1 is regulated by light-mediated degradation through the ubiquitin-26S proteasome pathway to optimize photomorphogenesis of seedlings in Arabidopsis. Plant J **44:** 1023–1035

Soy J, Leivar P, Monte E (2014) PIF1 promotes phytochrome-regulated growth under photoperiodic conditions in *Arabidopsis* together with PIF3, PIF4, and PIF5. J Exp Bot **65:** 2925–2936

Sturn A, Quackenbush J, Trajanoski Z (2002) Genesis: Cluster analysis of microarray data. Bioinformatics **18:** 207–208

Takano M, Kanegae H, Shinomura T, Miyao A, Hirochika H, Furuya M (2001) Isolation and characterization of rice phytochrome A mutants. Plant Cell **13:** 521–534

Tasaka M, Kato T, Fukaki H (1999) The endodermis and shoot gravitropism. Trends Plant Sci **4:** 103–107

Vitha S, Yang M, Sack FD, Kiss JZ (2007) Gravitropism in the *starch excess* mutant of *Arabidopsis thaliana*. Am J Bot **94:** 590–598

Wada M, Kong SG (2018) Actin-mediated movement of chloroplasts. J Cell Sci **131:** jcs210310

Wu X, Tang D, Li M, Wang K, Cheng Z (2013) Loose Plant Architecture1, an INDETERMINATE DOMAIN protein involved in shoot gravitropism, regulates plant architecture in rice. Plant Physiol **161:** 317–329

Yamamoto K, Kiss JZ (2002) Disruption of the actin cytoskeleton results in the promotion of gravitropism in inflorescence stems and hypocotyls of Arabidopsis. Plant Physiol **128:** 669–681

Yamauchi Y, Fukaki H, Fujisawa H, Tasaka M (1997) Mutations in the *SGR4, SGR5* and *SGR6* loci of *Arabidopsis thaliana* alter the shoot gravitropism. Plant Cell Physiol **38:** 530–535

Yang W, Ren S, Zhang X, Gao M, Ye S, Qi Y, Zheng Y, Wang J, Zeng L, Li Q, et al (2011) *BENT UPPERMOST INTERNODE1* encodes the class II formin FH5 crucial for actin organization and rice development. Plant Cell **23:** 661–680

Yano D, Sato M, Saito C, Sato MH, Morita MT, Tasaka M (2003) A SNARE complex containing SGR3/AtVAM3 and ZIG/VTI11 in gravity-sensing cells is important for *Arabidopsis* shoot gravitropism. Proc Natl Acad Sci USA **100:** 8589–8594

Zhang N, Yu H, Yu H, Cai Y, Huang L, Xu C, Xiong G, Meng X, Wang J, Chen H, et al (2018) A core regulatory pathway controlling rice tiller angle mediated by the *LAZY1*-dependent asymmetric distribution of auxin. Plant Cell **30:** 1461–1475

Zhang Z, Zhang Y, Tan H, Wang Y, Li G, Liang W, Yuan Z, Hu J, Ren H, Zhang D (2011) *RICE MORPHOLOGY DETERMINANT* encodes the type II formin FH5 and regulates rice morphogenesis. Plant Cell **23:** 681–700